Mirrorless buried waveguide laser in monoclinic double tungstates fabricated by a novel combination of ion milling and liquid phase epitaxy

Western Bolaños,[1,*] Joan J. Carvajal,[1] Xavier Mateos,[1] Ganapathy Senthil Murugan,[2] Ananth Z. Subramanian,[2] James S. Wilkinson,[2] Eugenio Cantelar,[3] Daniel Jaque,[3] Ginés Lifante,[3] Magdalena Aguiló,[1] and Francisco Díaz,[1]

[1]*Física i Cristal·lografia de Materials i Nanomaterials (FiCMA-FiCNA), Universitat Rovira i Virgili (URV), Campus Sescelades, c/Marcel·lí Domingo s/n 43007 Tarragona, Spain*

[2]*Optoelectronics Research Centre, University of Southampton, Highfield, Southampton, SO17 1BJ, UK*

[3]*Advanced Materials for Integrated Guided Optics (AMIGO), Departamento de Física de Materiales, Universidad Autónoma de Madrid, c/Francisco Tomás y Valiente no. 7, Ctra. Colmenar Viejo, km 15, 28049, Cantoblanco, Madrid, Spain*

**joanjosep.carvajal@urv.cat*

Abstract: Buried channel waveguides were fabricated by liquid phase epitaxial growth of a lattice-matched $KY_{0.58}Gd_{0.22}Lu_{0.17}Tm_{0.03}(WO_4)_2$ film on a microstructured $KY(WO_4)_2$ substrate. Channels were transferred to the substrates by standard photolithography and Ar-ion milling. The bottom and sidewalls of the milled channels were smooth enough (rms roughness = 70 nm and 20 nm, respectively) to favour the epitaxial growth of the active layer without defects at the boundary of substrate/epitaxial layer. The refractive index contrast was sufficient to enable light confinement and guided modes with low scattering losses were observed at wavelengths between 1440 nm and 1640 nm. CW laser operation at 1840 nm at room temperature was observed with feedback provided only by Fresnel reflection at the end faces, with slope efficiencies of 4% and 9% for TE and TM polarizations, respectively.

OCIS codes: (130.3130) Integrated optics materials; (140.3070) Infrared and far-infrared lasers; (140.3580) Laser, solid state; (230.7400) Waveguides, slab; (310.6845) Thin film devices and applications.

References and links

1. V. G. Kozlov, V. Bulovic, P. E. Burrows, and S. R. Forrest, "Laser action in organic semiconductor waveguide and double heterostructure devices," Nature **389**(6649), 362–364 (1997).
2. M. Sorel, P. J. R. Laybourn, G. Giuliani, and S. Donati, "Unidirectional bistability in semiconductor waveguide lasers," Appl. Phys. Lett. **80**(17), 3051–3053 (2002).
3. J. I. Mackenzie, C. Li, and D. Shepherd, "Multi-watt, high efficiency, diffraction-limited Nd:YAG planar waveguide laser," IEEE J. Quantum Electron. **39**(3), 493–500 (2003).
4. A. Rameix, C. Borel, B. Chambaz, B. Ferrand, D. P. Sheperd, T. J. Warburton, D. C. Hanna, and A. C. Tropper, "An efficient diode-pumped, 2 μm Tm:YAG waveguide laser," Opt. Commun. **142**(4-6), 239–243 (1997).
5. U. Griebner, and H. Schönnagel, "Laser operation with nearly diffraction-limited output from a Yb:YAG multimode channel waveguide," Opt. Lett. **24**(11), 750–752 (1999).
6. M. Hempstead, J. S. Wilkinson, and L. Reekie, "Wave-guide lasers operating at 1084 nm in neodymium-diffused lithium-niobate," IEEE Photon. Technol. Lett. **4**(8), 852–855 (1992).
7. P. Becker, R. Brinkmann, M. Dinand, W. Sohler, and H. Suche, "Er-diffused Ti:$LiNbO_3$ waveguide laser of 1563 nm and 1576 nm emission wavelengths," Appl. Phys. Lett. **61**(11), 1257–1259 (1992).
8. E. Cantelar, J. A. Sanz-García, G. Lifante, F. Cussó, and P. L. Pernas, "Single polarizad Tm^{3+} laser in Zn-diffused $LiNbO_3$ channel waveguides," Appl. Phys. Lett. **86**(16), 161119 (2005).
9. J. P. de Sandro, J. K. Jones, D. P. Shepherd, M. Hempstead, J. Wang, and A. C. Tropper, "Non-photorefractive CW Tm-in-diffused Ti:$LiNbO_3$ waveguide laser operating at room temperature," IEEE Photon. Technol. Lett. **8**(2), 209–211 (1996).
10. P. Rogin, and J. Hulliger, "Epitaxial Nd:YLF linear waveguide laser," Opt. Lett. **22**(22), 1701–1703 (1997).

#135469 - $15.00 USD Received 20 Sep 2010; revised 10 Nov 2010; accepted 12 Nov 2010; published 7 Dec 2010

11. E. Daran, D. P. Shepherd, T. Bhutta, and C. Serrano, "Laser operation of Nd:LaF_3 thin film grown by molecular beam epitaxy," Electron. Lett. **35**(5), 398–400 (1999).
12. P. M. Peters, D. S. Funk, A. P. Peskin, D. L. Veasey, N. A. Sanford, S. N. Houde-Walter, and J. S. Hayden, "Ion-exchanged waveguide lasers in Er^{3+}/Yb^{3+} codoped silicate glass," Appl. Opt. **38**(33), 6879–6886 (1999).
13. P. Madasamy, S. Honkanen, D. F. Geraghty, and N. Peyghambarian, "Single-mode tapered waveguide laser in Er-doped glass with multimode-diode pumping," Appl. Phys. Lett. **82**(9), 1332–1334 (2003).
14. A. Kahn, S. Heinrich, H. Kühn, K. Petermann, J. D. B. Bradley, K. Wörhoff, M. Pollnau, and G. Huber, "Low threshold monocrystalline Nd:$(Gd, Lu)_2O_3$ channel waveguide laser," Opt. Express **17**(6), 4412–4418 (2009).
15. H. Kühn, S. Heinrich, A. Kahn, K. Petermann, J. D. Bradley, K. Wörhoff, M. Pollnau, and G. Huber, "Monocrystalline $Yb(^{3+}):(Gd,Lu)(_2)O(_3)$ channel waveguide laser at 976.8 nm," Opt. Lett. **34**(18), 2718–2720 (2009).
16. Y. E. Romanyuk, C. N. Borca, M. Pollnau, S. Rivier, V. Petrov, and U. Griebner, "Yb-doped $KY(WO_4)_2$ planar waveguide laser," Opt. Lett. **31**(1), 53–55 (2006).
17. F. M. Bain, A. A. Lagatsky, S. V. Kurilchick, V. E. Kisel, S. A. Guretsky, A. M. Luginets, N. A. Kalanda, I. M. Kolesova, N. V. Kuleshov, W. Sibbett, and C. T. Brown, "Continuous-wave and Q-switched operation of a compact, diode-pumped Yb3+:KY(WO4)2 planar waveguide laser," Opt. Express **17**(3), 1666–1670 (2009).
18. S. Rivier, X. Mateos, V. Petrov, U. Griebner, Y. E. Romanyuk, C. N. Borca, F. Gardillou, and M. Pollnau, "Tm:$KY(WO(_4))(_2)$ waveguide laser," Opt. Express **15**(9), 5885–5892 (2007).
19. F. M. Bain, A. A. Lagatsky, R. R. Thomson, N. D. Psaila, N. V. Kuleshov, A. K. Kar, W. Sibbett, and C. T. A. Brown, "Ultrafast laser inscribed Yb:$KGd(WO_4)_2$ and Yb:$KY(WO_4)_2$ channel waveguide lasers," Opt. Express **17**(25), 22417–22422 (2009).
20. D. Geskus, S. Aravazhi, C. Grivas, K. Wörhoff, and M. Pollnau, "Microstructured $KY(WO(_4))(_2)$:$Gd(^{3+})$, $Lu(^{3+})$, $Yb(^{3+})$ channel waveguide laser," Opt. Express **18**(9), 8853–8858 (2010).
21. W. Bolaños, J. J. Carvajal, M. Cinta Pujol, X. Mateos, G. Lifante, M. Aguiló, and F. Díaz, "Epitaxial growth of lattice matched $KY_{1-x-y}Gd_xLu_y(WO_4)_2$ thin films on $KY(WO_4)_2$ substrates for waveguiding applications," Cryst. Growth Des. **9**(8), 3525–3531 (2009).
22. W. Bolaños, J. J. Carvajal, X. Mateos, M. C. Pujol, N. Thilmann, V. Pasiskevicius, G. Lifante, M. Aguiló, and F. Díaz, "Epitaxial layers of $KY_{1-x-y}Gd_xLu_y(WO_4)_2$ doped with Er^{3+} and Tm^{3+} for planar waveguide lasers," Opt. Mater. **32**(3), 469–474 (2010).
23. W. Bolaños, J. J. Carvajal, X. Mateos, M. Aguiló, and F. Díaz, "Exploring waveguiding properties of heavily doped Yb^{3+}:$KLu(WO_4)_2$ epitaxial layers," IEEE Photon. J. **2**(3), 482–489 (2010).
24. O. Silvestre, M. C. Pujol, R. Solé, W. Bolaños, J. J. Carvajal, J. Massons, M. Aguiló, and F. Díaz, "Ln^{3+}:$KLu(WO_4)_2$/ $KLu(WO_4)_2$ epitaxial layers:crystal growth and physical characterisation," Mater. Sci. Eng. B **146**(1-3), 59–65 (2008).

1. Introduction

The development of waveguide lasers (WLs) for integrated optics using novel materials is under intense investigation. Using WLs instead of bulk lasers brings the following advantages: i) the reduction of the cavity mode-volume due to the optical confinement in the active host, ii) high optical gain, iii) low laser thresholds and iv) the laser cavity may be contained in the thin active film, allowing on-chip integration of these WLs with other optical components. In addition to semiconductors [1,2], several rare earth doped materials have demonstrated their potential for operation as WLs, such as oxides [3–9], fluorides [10,11], glasses [12,13], sesquioxides [14,15] and more recently monoclinic double tungstates, $KRE(WO_4)_2$ (or KREW, for short, where RE = Y, Gd and Lu) [16–20].

KREWs have emerged as promising materials for the fabrication of WLs mainly because they: (i) exhibit large values of absorption and emission cross sections for the rare earth ions, allowing high gain to be obtained and hence low-threshold laser operation; (ii) possess large ion to ion distance, which allows high doping levels of the active ions without the quenching of fluorescence; and (iii) have high refractive index values of about 2.0, which makes them suitable for the fabrication of compact integrated optical devices. In this direction, advances in KREW slab and channel waveguide lasers activated with rare earths have recently been reported. As slab waveguides, for instance, laser operation of Yb^{3+} doped: $KY(WO_4)_2$ [16,17] and Tm^{3+} doped $KY(WO_4)_2$ [18] has been demonstrated. On the other hand, laser action of buried channel waveguides fabricated by ultrafast laser writing on Yb: $KGd(WO_4)_2$ and Yb: $KY(WO_4)_2$ were reported by Bain et al. [19] and Geskus et. al. have reported on the laser action of Gd^{3+}, Lu^{3+} and Yb^{3+} co-doped $KY(WO_4)_2$ channel waveguides structured by Ar ion beam milling [20].

Through a systematic study [21], we determined the optimum composition of a $KY_{1-x-y}Gd_xLu_y(WO_4)_2$ film which exhibits both low lattice mismatch and high refractive index contrast with the $KY(WO_4)_2$ substrate. This composition, corresponding to a

#135469 - $15.00 USD Received 20 Sep 2010; revised 10 Nov 2010; accepted 12 Nov 2010; published 7 Dec 2010

$KY_{0.59}Gd_{0.19}Lu_{0.22}(WO_4)_2$ layer was successfully grown by liquid phase epitaxy on a $KY(WO_4)_2$ substrate without cracking and with a refractive index contrast with the substrate of the order of 2×10^{-3} at $\lambda = 632.8$ nm, allowing the demonstration of passive waveguiding with scattering losses ~1 dB/cm. Our lattice matched layer was activated with Tm^{3+} maintaining the high structural quality and the refractive index contrast [22]. However, the concentration was too low to obtain laser operation.

In this paper we report a new method for the fabrication of buried channel waveguides on monoclinic double tungstates ($KY(WO_4)_2$) that combines standard UV photolithography, Ar^+–ion milling and Liquid Phase Epitaxial growth (LPE) of a lattice matched $KY_{0.58}Gd_{0.22}Lu_{0.17}Tm_{0.03}(WO_4)_2$ layer. This was followed by the growth of a cladding layer of $KY(WO_4)_2$ by LPE on top of the active layer. This new materials technology has enabled us to fabricate what we believe is the first Tm^{3+} doped monoclinic double tungstate channel waveguide laser emitting at 1.8 μm without the need for end-butted mirrors.

2. Experimental methods

$KY(WO_4)_2$ substrates were obtained from $KY(WO_4)_2$ bulk crystals grown by high temperature Top Seeded Solution Growth (TSSG) in a vertical tubular furnace. While rotating at 42 rpm, a **b** –oriented seed [21] was placed in contact with the surface of the solution (solute/solvent ratio 12:88 mol%) in order to determine the saturation temperature, T_s, i.e. the temperature at which neither growth nor dissolution of the seed is observed. Once T_s was determined, the growth process started by slowly cooling the solution at 0.12 K/h until 30 K below T_s. More details on the growth conditions and setup can be found in [21–23]. The $KY(WO_4)_2$ bulk crystals were then cut into ~2 mm thick plates perpendicular to the **b** –direction. Finally, both sides of each plate were polished with 9 μm, 3 μm, 1 μm and 0.3 μm alumina powders to achieve high quality polishing of the substrates with an average radius of curvature of 80 m and roughness as low as 34 nm.

For measuring the Ar^+ ion milling rates, a Rohm & Haas S1828 photoresist layer was spun and soft baked onto a piece of KYW substrate. For microstructuring the substrates we used the same photoresist and a dark field mask with channels of different widths ranging from 1 μm to 10 μm, at an interval of 0.2 μm and with 100 μm spacing between each waveguide. The channel pattern was transferred to the photoresist by standard UV photolithography. After that, we transferred this pattern to the substrates by Ar ion milling in an Oxford Plasma Technology Ionfab 300 plus system using an Ar^+ ion beam accelerated at 300 V with a beam current of 100 mA. The samples were mounted on a cooled plate (288.5 K) held at 45°, which rotated at 5 rpm for the duration of etching.

$KY_{0.58}Gd_{0.22}Lu_{0.17}Tm_{0.03}(WO_4)_2$ layers were grown on the microstructured substrates by LPE using a solution prepared with the solute:solvent ratio 7:93 mol % since this solution composition allows for a better control on the growth rate of the epitaxial layers [24]. Once more, T_s was accurately determined for this solution using a **b** –oriented seed in the same way as it was determined for the bulk crystal growth. Subsequently, the substrate with the microchannels inscribed in one face was partially immersed into the solution at T_s by vertical dipping. Immediately after immersion, we induced the supersaturation of the solution by suddenly decreasing the temperature to 3 K below T_s and the epitaxial growth process then progressed for 3 hours at this temperature. Finally the substrate was removed from the solution and the furnace was cooled to room temperature at a rate of 15 K/h preventing cracking of the structures by thermal shock. After polishing this epitaxial layer to a thickness of 2 μm over the non-structured surface of the substrate, an overcladding layer of $KY(WO_4)_2$ was grown by LPE, using the same growth conditions as those given above.

The chemical composition of the bulk single crystals and the epilayers was determined by Electron Probe Microanalysis (EPMA) with a CAMECA SX 50 instrument. The measurements were performed with a beam current of 20 mA, an acceleration voltage of 20 kV, over 10 s for measuring oxygen, potassium, yttrium and tungsten, and over 30 s for measuring gadolinium, lutetium and thulium.

#135469 - $15.00 USD Received 20 Sep 2010; revised 10 Nov 2010; accepted 12 Nov 2010; published 7 Dec 2010

The three refractive indices of the substrate and of the $KY_{0.58}Gd_{0.22}Lu_{0.17}Tm_{0.03}(WO_4)_2$ epitaxial layer were measured by means of a Metricon 2010 prism-film coupler system at λ = 632.8 nm and λ = 1523 nm. In both cases the TE polarization yielded measurements of the refractive indices n_g and n_m, associated with the $\boldsymbol{N_g}$ and $\boldsymbol{N_m}$ principal optical directions, respectively, while the TM polarization was used to determine the refractive index n_p, associated with the third principal optical direction, $\boldsymbol{N_p}$, which is perpendicular to $\boldsymbol{N_g}$ and $\boldsymbol{N_m}$

3. Results and discussion

The as-grown bulk $KY(WO_4)_2$ single crystals were crack and macrodefect free and had a typical mass of about 10 g with average dimensions around 9 × 20 × 9 mm^3 along the a* × c × b crystallographic directions. Substrates for microstructuring and epitaxial growth were cut from $KY(WO_4)_2$ bulk crystals. Figure 1 shows a photograph of a typical **b**–oriented $KY(WO_4)_2$ substrate after polishing, indicating the location of the optical frame with respect to the crystallographic frame in these monoclinic crystals. Monoclinic double tungstates are biaxial crystals. The binary axis of symmetry of these crystals is parallel to the **b** crystallographic direction, which is also parallel to one of the three principal optical directions. The principal optical directions are labeled $\boldsymbol{N_g}$, $\boldsymbol{N_m}$ and $\boldsymbol{N_p}$. The $\boldsymbol{N_g}$ and $\boldsymbol{N_m}$ optical directions are located in the **a**-**c** crystallographic plane whilst the $\boldsymbol{N_p}$ optical direction is perpendicular to that plane and is parallel to the **b** crystallographic direction. For $KY(WO_4)_2$ the $\boldsymbol{N_g}$ optical direction is located at 18.5° clockwise from the **c** crystallographic axis and hence, the $\boldsymbol{N_m}$ optical direction (which is perpendicular to $\boldsymbol{N_g}$) is located at an angle of 59.2° with respect to the **a** crystallographic axis [23].

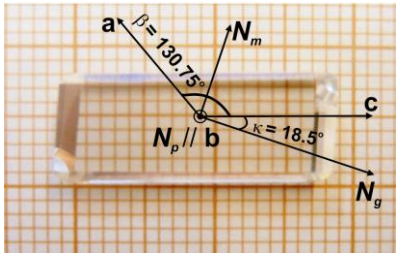

Fig. 1. b –oriented $KY(WO_4)_2$ substrate used for microstructuring and epitaxial growth.

We tested the possibility of structuring $KY(WO_4)_2$ substrates by using Reactive Ion Etching (RIE) with CHF_3 and SF_6 gases, yielding an etch rate of 200 nm/h, which was too low for practical purposes. We then explored Ar-ion beam milling. A 4 μm thick photoresist (PR) film was spun onto a $KY(WO_4)_2$ substrate. The system (PR + substrate) was exposed to the Ar- ion beam for different etching times. In this way we determined the etch rate as can be seen in Fig. 2. The etch rates obtained with Ar^+- ion beam milling were 1.13 μm h^{-1} for the substrate and 1.01 μm h^{-1} for the PR. We therefore selected this method due to its improved etch rates and acceptable selectivity for structuring the $KY(WO_4)_2$ substrates.

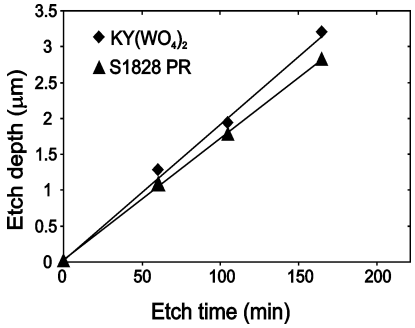

Fig. 2. Etch depth by Ar- ion milling as a function of etch time for $KY(WO_4)_2$ and photoresist.

#135469 - $15.00 USD Received 20 Sep 2010; revised 10 Nov 2010; accepted 12 Nov 2010; published 7 Dec 2010

After spinning an 8 μm thick film of photoresist in two stages onto the $KY(WO_4)_2$ substrates, straight channels were patterned on the photoresist using standard UV photolithography. Since the $\boldsymbol{N_m}$ principal optical direction exhibits the highest absorption and emission cross sections in the monoclinic double tungstates, the photolithographic mask was carefully aligned in such a way that the channels were parallel to the $\boldsymbol{N_g}$ principal optical direction of the substrate, so that we could take advantage of the high absorption cross-section of the Tm^{3+} ions along $\boldsymbol{N_m}$ by coupling the light in the horizontal (TE) polarization; TM propagating modes could also be excited in these channels.

According to the etch rates found, and after developing the UV exposed PR, the substrate patterned with PR was exposed to the Ar^+ –ion beam for 7 hours leading to channels with the shape and dimensions shown in Fig. 3(a) and 3(b), as characterized by an optical imaging profiler.

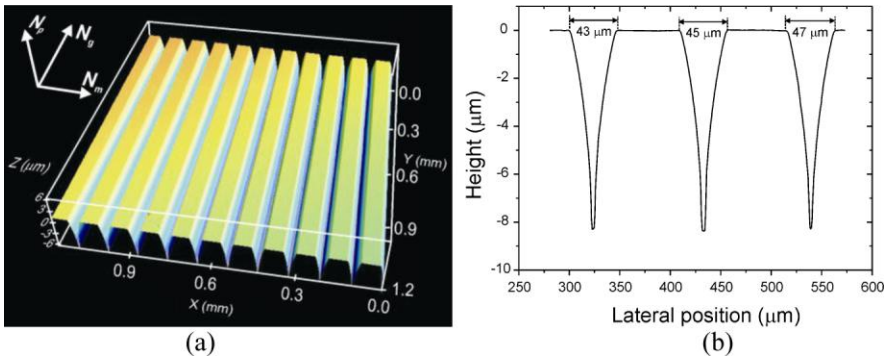

Fig. 3. (a) Topography, and (b) extended profiles of some typical channels milled on $KY(WO_4)_2$ substrate.

Figure 3 shows that etched channels with trapezoidal cross-sections were obtained. The channels all had depths of 6 ± 2 μm and the different widths on the mask resulted in only different widths at the top [see Fig. 3(b)]. The sidewalls of the channels exhibited a mean rms roughness of 20 nm, whereas on the bottom the roughness was 70 nm, comparable to the roughness usually achieved by the mechanical polishing process of the substrates, 34 nm, which is a key factor to obtain a high quality epitaxial layer and to minimize the scattering losses generated by defects at the interface between the substrate and the epitaxial layer. Light confinement and waveguide lasing in the trapezoidal cross-section waveguides were observed, as discussed below.

A crack free and macroscopic defect free layer of $KY_{0.58}Gd_{0.22}Lu_{0.17}Tm_{0.03}(WO_4)_2$ grown on the ion-milled **b**–oriented $KY(WO_4)_2$ substrate was obtained by LPE. The typical thickness of the as-grown epilayer was about 50 μm, as can be seen in the cross sectional Environmental Scanning Electron Microscopy (ESEM) image of the epitaxial layers, shown in Fig. 4(a), and recorded by using backscattered electrons. The chemical composition of the epitaxial layer was measured by EPMA, and the Tm^{3+} ion concentration was found to be 1.75×10^{20} cm^{-3}. The epitaxial layer adapted perfectly to the morphologies induced by the Ar^+-ion milling process on the substrate, filling all the space. No defects were observed at the interface between the substrate and the epitaxial layer.

#135469 - $15.00 USD Received 20 Sep 2010; revised 10 Nov 2010; accepted 12 Nov 2010; published 7 Dec 2010

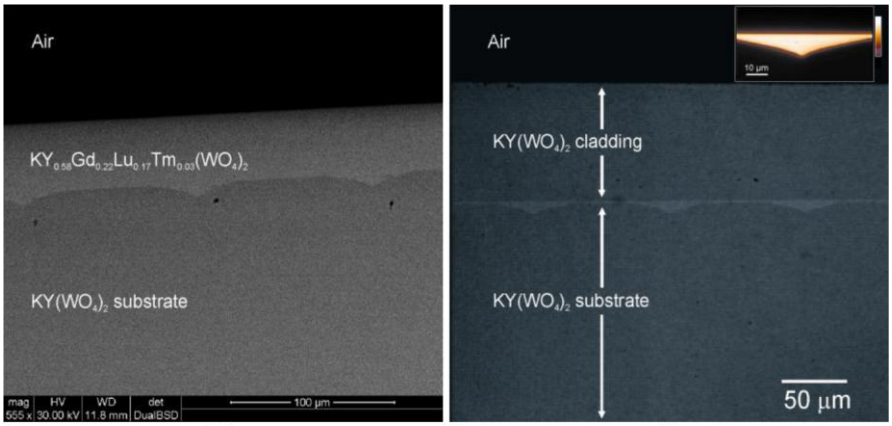

Fig. 4. Cross-sectional views of (a) epitaxial growth over microstructured channels in the $KY(WO_4)_2$ substrate, and (b) $KY(WO_4)_2/KY_{0.58}Gd_{0.22}Lu_{0.17}Tm_{0.03}(WO_4)_2/KY(WO_4)_2$ buried rib waveguides. Inset shows the Tm^{3+} luminescence map taken with a confocal microscope.

The as-grown epitaxial layer was polished down to a height of ~2 μm with respect to the unmilled surface of the substrate. This led to an inverted rib-like active layer over the grooves of the ion-milled substrate. After that, a 70-μm thick $KY(WO_4)_2$ cladding was grown by LPE over the $KY_{0.58}Gd_{0.22}Lu_{0.17}Tm_{0.03}(WO_4)_2$ epilayer [see Fig. 4(b)]. The lighter region in Fig. 4(b) corresponds to the active layer, which shows a contrast to the substrate and cladding due to its different chemical composition. This layer forms the buried rib waveguides. The sharp contrast observed in the image between the active layer and the substrate or the cladding shows that there is no diffusion of the ions from the epilayer into the substrate/cladding or from the substrate/cladding into the active layer. The Tm^{3+} luminescence image shown in the inset also confirms that there is no significant diffusion of active ions from the guiding layer into the substrate or cladding.

Prior to the polishing of the active layer and growth of the cladding layer, we measured the three refractive indices n_g, n_m, and n_p of the active guiding layer and the $KY(WO_4)_2$ substrate at different wavelengths (632.8 nm and 1523 nm) by the prism- film coupling technique. With this setup we also observed the guided modes supported by the guiding layer. Table 1 summarizes the results of these measurements.

Table 1. Refractive indices of the substrate and a 12 μm thick $KY_{0.58}Gd_{0.22}Lu_{0.17}Tm_{0.03}(WO_4)_2$ guiding layer measured by the prism-film coupling technique

		Substrate	Guiding layer (slab)
λ (nm)	**Optical Direction**	**Refractive index**	**Refractive Index**
632.8	N_g	2.0854	2.0910
	N_m	2.0405	2.0445
	N_p	1.9976	2.0021
1523	N_g	2.0380	2.0437
	N_m	1.9965	2.0021
	N_p	1.9587	1.9662

The refractive index contrasts at 632.8 nm and 1523 nm were of the order of 10^{-3}, high enough to enable guided light along the three principal optical directions, especially in the N_m and the N_p directions, which are the directions along which light may be polarized in the fabricated buried ribs. Seven and six TE guided modes were supported by a 12 μm-thick planar waveguide along the N_g and N_m optical directions, respectively, at 632.8 nm, whereas,

#135469 - $15.00 USD Received 20 Sep 2010; revised 10 Nov 2010; accepted 12 Nov 2010; published 7 Dec 2010

at this wavelength seven TM modes were supported along the N_p optical direction. At 1523 nm, the number of guided modes decreased, as expected, up to two TE modes along the N_g and N_m optical directions and three TM modes along the N_p optical direction.

Guided modes supported by the buried channel waveguides were also observed using a CCD camera at a wavelength of 1640 nm, far from any absorption band of the active ion, for channel waveguides of different widths. Light was coupled into the waveguides through a 150 μm core fiber. Figure 5 shows the near-field mode intensity profile of a typical 30 μm width channel waveguide. The intensity profile corresponding to the fundamental mode shown in Fig. 5 was fitted to a Gaussian distribution in the vertical and horizontal directions, yielding a measured spot size (e^{-2} half-widths) of 8 × 47 μm^2.

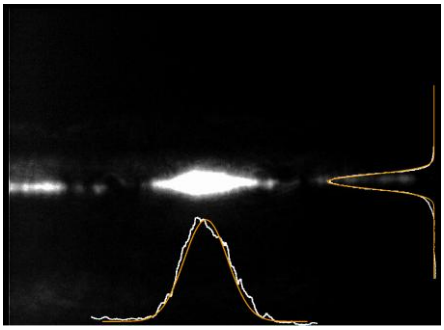

Fig. 5. Mode intensity distribution of a $KY_{0.58}Gd_{0.22}Lu_{0.17}Tm_{0.03}(WO_4)_2$ buried rib waveguide taken at 1640 nm.

Losses in our 10 mm long channel waveguides were evaluated by measuring the transmitted light at 633 nm, using a 5 × objective microscope for light injection in the waveguide and collecting the output power by a 10 × microscope objective. At this wavelength the channel waveguide is multimode, and the doped core is free of absorption from the Tm^{3+} ions. Assuming a 100% coupling efficiency and taking into account the Fresnel losses (11%) at the air/waveguide interfaces, the upper limit for losses was evaluated, giving a value of 0.2 dB/cm for both quasi-TE and quasi-TM propagating light. This low value of losses is an indicative of the quality of the layers grown by the LPE. Furthermore, since the scattering losses at the waveguide interfaces strongly depend on the index contrast, the epitaxially grown over-cladding helps favorably to reduce these losses.

Laser operation of the transition from the $^3F_4 \rightarrow {}^3H_6$ levels of Tm^{3+} in the continuous wave regime at room temperature was obtained in several buried channel waveguides. The pump source used was an argon-ion laser pumped Ti:Sapphire laser operating at 802 nm. Long working distance microscope objectives of 10 × and 50 × were used for in-coupling and out-coupling the pump and the laser signal to and from the waveguides, respectively, which provided a pump spot size of ~64 μm. The feedback provided by the 11% Fresnel reflections at the end faces alone was sufficient to enable laser oscillation, and allowing us to operate a mirrorless guided laser. Laser characteristics of a representative channel are shown in Fig. 6(a) and 6(b).

#135469 - $15.00 USD Received 20 Sep 2010; revised 10 Nov 2010; accepted 12 Nov 2010; published 7 Dec 2010

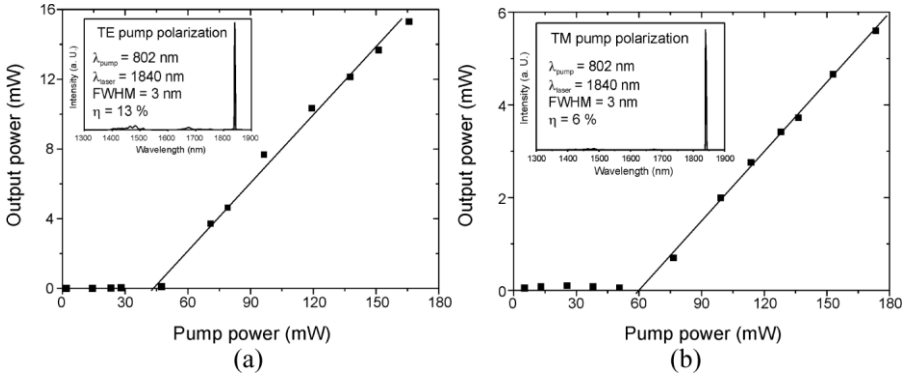

Fig. 6. CW output power versus pump power at room temperature of a $KY_{0.58}Gd_{0.22}Lu_{0.17}Tm_{0.03}(WO_4)_2$ buried rib waveguide for two different polarizations without mirrors: (a) TE pump polarization, with electric field parallel to N_m optical direction, and (b) TM pump polarization with magnetic field parallel to N_p optical direction. Insets show the emission spectra in the range 1300 nm – 1900 nm.

Slope efficiencies as high as 13% were achieved for the TE pump polarization, whilst for the TM polarization the maximum slope efficiency was 6% with a laser thresholds of 42 mW and 60 mW, respectively. The FWHM in both cases was 3 nm. These efficiencies are considerably larger than those reported in Tm:$LiNbO_3$ waveguide lasers (around 1%) [8,9] As expected, higher laser efficiencies for TE pump polarization due to the high absorption and emission cross sections for this polarization were obtained. However, we observed blue emission generated by up-conversion processes during the lasing experiments ($^1G_4 \rightarrow {}^3H_6$ centred at 480 nm) that could be considered as a competitive source for the laser efficiencies.

4. Conclusion

In conclusion, we have developed a novel method for the fabrication of buried channel waveguides in monoclinic double tungstates. In summary, the method consists of (i) manufacturing channels on $KY(WO_4)_2$ substrates by standard UV photolithography and Ar^+-ion milling and (ii) liquid phase epitaxial growth of a lattice matched layer over the milled $KY(WO_4)_2$ substrates. The guiding layer grown into the channels was activated with Tm^{3+}. Its chemical composition was $KY_{0.58}Gd_{0.22}Lu_{0.17}Tm_{0.03}(WO_4)_2$, with an active ion concentration of 1.75×10^{20} cm^{-3}. A refractive index contrast of the order of 10^{-3} with respect to the substrate was sufficient to observe highly confined guided light at different wavelengths, in particular, in the range 1440 nm–1640 nm. The feedback provided by Fresnel reflection at the end-faces enabled the demonstration of CW laser operation at 1840 nm for the first time in this family of materials when pumped at 802 nm, with efficiencies of 13% and 6% for TE and TM pump polarizations, respectively, allowing the demonstration of a mirrorless guided laser. We believe that this new technology can be easily extended to other dielectric materials. WLs emitting in the spectral region around 2 μm, as well as solid state lasers, are in demand and will be highly useful in mid-IR molecular finger printing applications, including remote sensing, gas detection, high resolution molecular spectroscopy, frequency metrology, but also in medicine, since characteristic vibrational absorption lines of molecular species of interest in these fields are located in this spectral region.

Acknowledgments

This work was supported by the Spanish Government under projects MAT 2008-06729-C02-02/NAN, PI09/90527 and TEC2010-21574-C02-02 and the Catalan Government under project 2009SGR235. W. Bolaños also thanks the Catalan Government for the funds provided through the Fellowship 2009FI_B 00626. J. J. Carvajal is supported by the Research and Innovation Ministry of Spain and European Social Fund under the Ramón y Cajal program,

#135469 - $15.00 USD Received 20 Sep 2010; revised 10 Nov 2010; accepted 12 Nov 2010; published 7 Dec 2010

RYC2006-858. The authors would like to express their gratitude to Neil Sessions and David Sager for their technical advice and contributions.

#135469 - $15.00 USD Received 20 Sep 2010; revised 10 Nov 2010; accepted 12 Nov 2010; published 7 Dec 2010